2023 IEEE Biomedical Circuits and Systems Conference (BioCAS) | 979-8-3503-0026-0/23/$31.00 ©2023 IEEE | DOI: 10.1109/BioCAS58349.2023.10388693

Artificially-Intelligent Fascicle-Selective Bidirectional Peripheral Nerve Interfaces

Jianxiong Xu, Jose De Sales Filho, Eugene Hwang, Sudip Nag, Liam Long,
Mustafa Kanchwala, Mohammad Abdolrazzaghi, Yu Huang, Jose Zariffa, Roman Genov
University of Toronto, Toronto, ON, CA
jianxiong.xu@mail.utoronto.ca, roman@eecg.utoronto.ca

***Abstract*—This paper presents a comprehensive overview of our latest work on two design strategies for minimally invasive, battery-free wireless neural interfaces for adaptive neuromodulation therapy in the peripheral nervous system (PNS). These active PNS neural interfaces provide alternative treatment options for patients with motor, sensory and other neurological deficits, aiming to improve their quality of life. Each of the two presented designs includes a nerve-scale integrated circuit (IC) performing fascicle-selective extraneural recording and stimulation. For fascicle-selective neural recording, the IC interacts wirelessly with a wearable interrogator which performs machine-learning inference on the recorded neural signals. For fascicle-selective neuro-stimulation, two techniques - subthreshold current pulses and temporal interference stimulation methods are adopted. Two oversampling neural ADC architecture choices are also compared: an energy-efficient passive 2nd-order delta-sigma ADC and a high-resolution noise-shaping SAR ADC. Inductive and ultrasound energy harvesting for wireless powering and data reception are also discussed. In vivo results from rodent studies are included to support the validity of the discussed design strategies.**

***Index Terms*—Peripheral Nervous System, Neural Interfaces, Fascicle-Selective Neural Recording, Fascicle-Selective neuro-stimulation, Delta-Sigma ADC, Noise-Shaping SAR ADC, Wireless Powering**

I. Introduction

The peripheral nervous system (PNS) plays an integral role in establishing a communicative link between various organs and the central nervous system. Innovations in miniature electronic PNS interfaces that monitor and modulate neural activity in peripheral nerves have been instrumental in propelling medical advancements, particularly in the restoration of motor and sensory capabilities for those suffering from paralysis or amputation. Furthermore, such PNS interface technologies have been leveraged in the development of implantable closed-loop therapeutic devices, which mark a significant breakthrough in the management of chronic medical conditions linked to autoimmune or metabolic disorders [1].

However, there are still numerous obstacles preventing the effective and widespread deployment of PNS neural interfaces: (1) the invasiveness of the requisite cables, electronics, and batteries; (2) sub-optimal control of nerve fascicle selectivity; and (3) a lack of patient-specific adaptability. Conventional nerve cuff electrodes, depicted in Fig. 1(a), utilize tripolar recording, which is plagued by multiple notable disadvantages. These include: (1) vulnerability to mechanical failure, (2) increased susceptibility to electromagnetic interference,

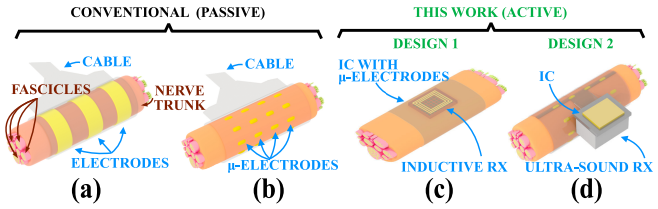

Fig. 1. Comparative illustrations of PNS neural interfaces. (a) Conventional tripolar recording nerve cuff. (b) Conventional high-density electrodes on flexible nerve cuff. (c) Design 1: Die-on-cuff active interface [2]. (d) Design 2: Flexible-rigid active interface [3].

which deteriorates the signal-to-noise ratio (SNR), and (3) a substantial implant form factor that escalates invasiveness and cost. Additionally, the requirement for minimal recurring battery replacements amplifies the device's size. Despite the tripolar configuration's capacity to reduce artifacts stemming from adjacent muscle activity or stimulation, it remains acutely sensitive to cuff impedance imbalance and fails to offer fascicle selectivity. Passive high-density flexible nerve cuffs, illustrated in Fig. 1(b), may augment selectivity but are not exempt from the other inherent limitations of the passive configuration.

We present two of our most recent designs of PNS neural interfaces devised to mitigate these challenges: both are battery-free wireless PNS interfaces with individual fascicle selectivity. At the core of each of these designs is a miniature system-on-chip integrated circuit (IC) with extraneural recordering and stimulation capabilities. These ICs are complemented by a wearable RFID-style interrogator equipped with a machine learning edge-inference engine. It enables a fascicle-selective neuromodulation therapy approach without the need for risky invasive procedures on the nerve trunk, such as intrafascicular [4] or regenerative [5], [6] implantation into the nerve truck.

The first design involves flip-chip bonding IC onto a petite electrode array cuff clip, as displayed in Fig. 1(c). Minimal compression is exerted on the nerve to ensure optimal planar array contact, akin to the passive FINE electrodes routinely implanted in humans [7]. The second design, depicted in Fig. 1(d), embeds the IC onto the rigid section of a flexible-rigid electrode array substrate. This pliable electrode array accommodates the nerve's shape, effectively enveloping it to minimize the probability of nerve damage. The wireless functionality of the proposed devices is enabled by inductive

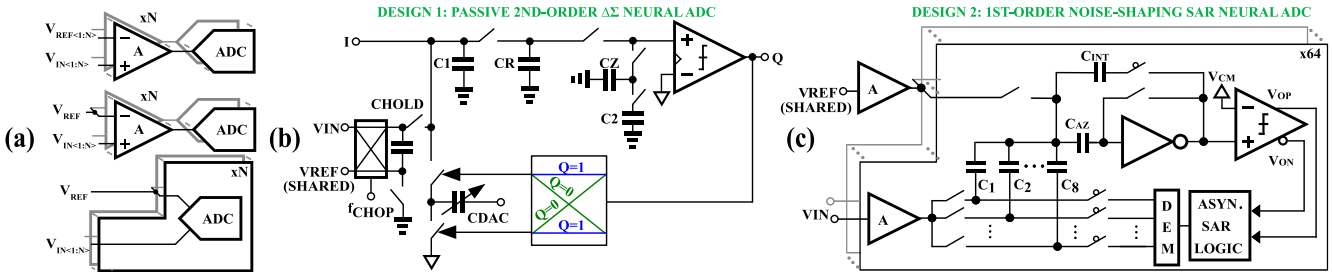

Fig. 2. (a) Top-to-bottom: bipolar differential recording, unipolar differential recording, and unipolar pseudo-differential recording configurations. (b-c) Two implementations of unipolar pseudo-differential PNS neural interfaces: (b) power-efficient passive 2nd-order $\Delta\Sigma$ neural ADC [2], and (c) high-resolution 1st-order noise-shaping (NS) SAR neural ADC [3].

power and ultrasonic power transmission, respectively. This attribute facilitates deeper implantation of the device, abolishes the necessity for obtrusive cables, and significantly reduces the invasiveness of the implantation process. By situating the recording system adjacent to the recording site, the SNR is significantly enhanced, and the influence of electromagnetic interference is diminished, ultimately improving the overall interface performance.

Each of the two proposed PNS interfaces attains fine deep fascicle selectivity without necessitating nerve penetration. For fascicle-selective neurostimulation, inspired by the work in the central nervous system [8], [9], the first design adopts the non-overlapping subthreshold current pulses method [8] and the second design adopts the temporally interfering electric field method [9] to selectively stimulate individual fascicles, respectively. For fascicle-selective recording, a digital convolutional neural network (CNN) classifier has been employed to perform online edge-inference on the recorded neural data.

II. Fascicle-Selective Recording

This section introduces design choices for the analog-front architecture and the digital CNN classifier architecture. With these, the proposed PNS neural interface achieves selective recording.

A. Analog-front end architecture

As depicted in Fig. 2(a, top), one choice for neural amplifiers is to employ bipolar differential recording [10]–[12] for high common-mode rejection ratio (CMRR) at the cost of requiring a larger number of electrodes, which increases the size, complexity and cost of neural interfaces. In addition, if the recording area is constrained, an increased number of electrodes may also result in a smaller distance between electrodes and a smaller electrode size, leading to recorded signal degradation. Unipolar differential recording (Fig. 2(a, middle)) [13], [14] is therefore favored. It offers enhanced signal amplitude, but suffers from a large mismatch in the input impedance leading to degraded CMRR. We employ a pseudo-differential configuration that overcomes these limitations (Fig. 2(a, bottom)).

Our first pseudo-differential design [2] incorporates a power-optimized 2nd-order $\Delta\Sigma$ ADC, as seen in Fig. 2(b). It substitutes the energy-intensive operational transconductance

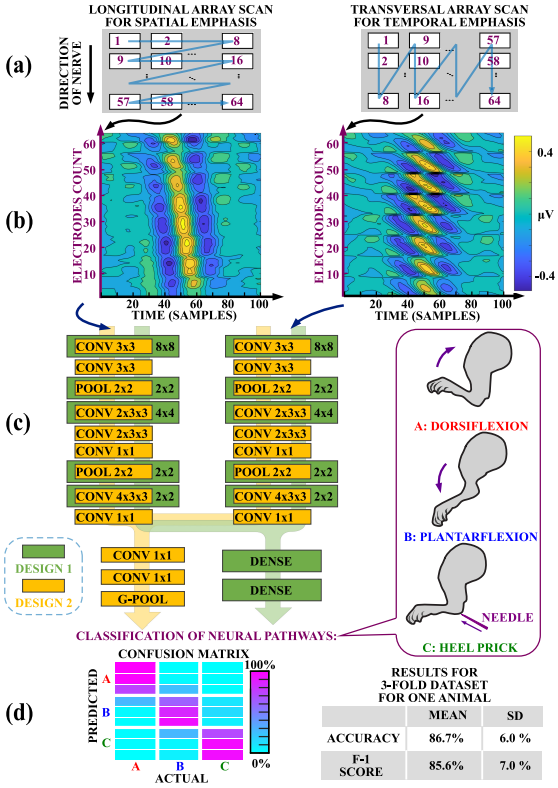

Fig. 3. Fascicle-selective neural recording strategy. (a) A method of reorganizing the digital neural data from an 8×8 electrode array to an 64×100 spatiotemporal feature matrix. (b) Depiction of the 64×100 spatiotemporal feature matrix formed from the reorganized digital neural data by rows (left) and columns (right), to emphasize spatial and temporal features, respectively. (c) Two versions of the inference engine that classifies the neural activity into one of the three classes: dorsiflexion, plantarflexion, and heel prick. Designs 1 and 2 employ the models highlighted in green and yellow, respectively. The yellow implementation provides resource-efficient neural networks with minimal accuracy loss compared to the green version. It is suitable for resource-constrained implantable hardware and requires significantly fewer weights, memory, and FLOPs. Despite this, it maintains F-1 score above 0.85. (d) The best (yellow) classifier's performance results, including accuracy and F-1 score, derived from a 3-fold dataset.

amplifier and integrator, typically found in the majority of $\Delta\Sigma$ ADCs, with an opamp-less charge pump and passive integrators that are more power-efficient. Furthermore, this configuration enables the frequency multiplexing of differential neural voltage, $(V_{IN} - V_{REF})$, and base-band cur-

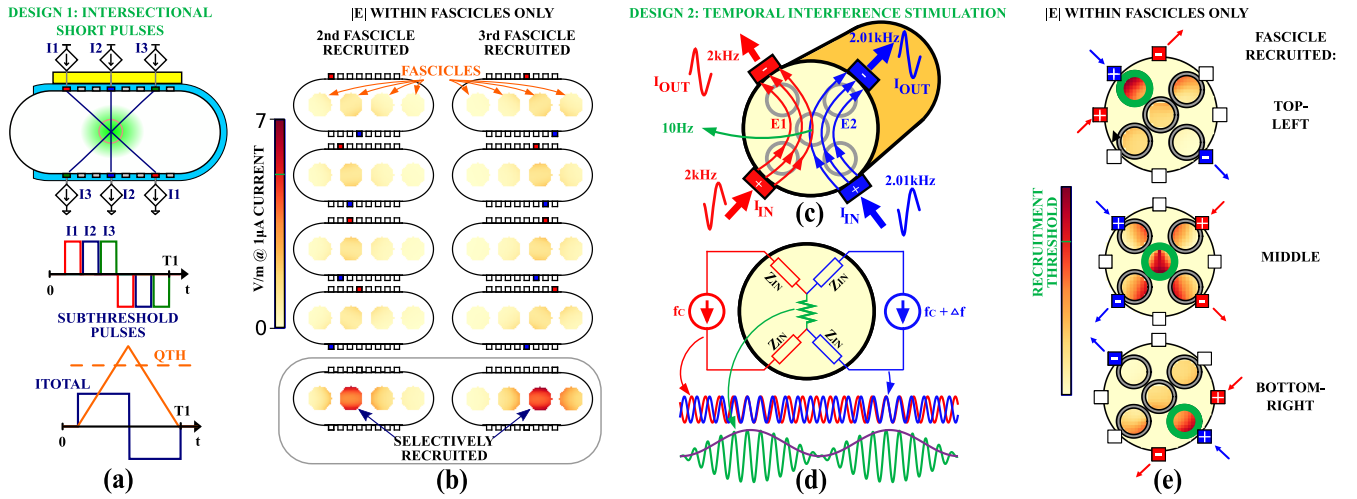

Fig. 4. Fascicle-selective neural stimulation strategies. (a) Selected fascicle recruitment by the intersectional short pulses method [2]. (b) FEM simulation of targeted stimulation by the intersectional short pulses method. (c) & (d) Temporal interference stimulation (TIS) method example and its principle of operation, respectively [3]. (e) TIS method's selective stimulation capability illustrated by a FEM simulation.

rent, I, which facilitates simultaneous voltage and electrode impedance recording. The CMRR is primarily constrained by the mismatch of the input impedance and the discrepancies between the top and bottom plates of the sampling capacitor. Nonetheless, despite these constraints, the design maintains an adequate CMRR for a PNS interface.

In our second pseudo-differential design [3], we introduce an additional preamplifier to an ADC to enhance the input impedance matching such that it upholds an improved CMRR, as illustrated in Fig. 2(c). Each of these preamplifiers exploits a switched-capacitor correlated-double-sampling amplifier, which is aimed at mitigating low-frequency noise and offset. A first-order NS-SAR ADC with an inverter-based integrator conducts differential sampling of the pre-amplified neural and reference signals, thereby enabling moderate common-mode rejection. Moreover, the implementation of asynchronous SAR logic facilitates rapid conversion. Concurrently, the design employs dynamic element matching (DEM) to minimize the implications of mismatch within the capacitor bank.

B. Digital convolutional neural network classifier

We deploy a CNN to link naturally-evoked compound action potentials (nCAP) we record with specific neural pathways using spatiotemporal patterns, as shown in Fig. 3, which involves the following steps:

1) nCAP detection: The recorded signals are averaged to enhance the SNR. Subsequently, nCAPs are detected by applying a thresholding method to this averaged signal.

2) Spatiotemporal signature extraction: Once nCAPs are identified, the spatiotemporal signatures are established by reorganizing the 8×8 digital neural data, both longitudinally and transversely (Fig. 3(a)), emphasizing spatial and temporal features forming two 64×100 matrixes as shown in Fig. 3(b).

3) Training: The extracted spatiotemporal signatures are then used to train a CNN model with Tensorflow Keras libraries using stochastic gradient descent optimization and categorical cross-entropy loss. Training included 1000 epochs or whenever the validation loss function did not decrease for over 15 epochs.

4) Inference: The CNN classifier then associates each nCAP with a specific neural pathway (dorsiflexion, plantarflexion, and heel pricking) as shown in Fig. 3(c).

This algorithm was initially proposed in [15] and subsequently improved to be implemented in wearable hardware in our first design [2], [16] (green in Fig. 3(c)). To accommodate CNNs on even smaller wearable devices, our second design was further improved [17] (yellow in Fig. 3(c)). The main modification is that fully connected output layer is replaced with two convolutional layers and a global pooling layer, drastically reducing filter parameters by a factor of 420, yet only slightly decreasing F-1 score performance. Results in Fig. 3(d) show the classifier's accuracy at 86.7% and its F-1 score at 85.6% from a 3-fold dataset derived from a single animal.

III. Fasicle-Selective Stimulation

Our first design adapts intersectional short pulses (ISP) method [8], initially developed for the brain, to the PNS (Fig. 4 (a)), to stimulate individual deep fascicles selectively. The intersectional short pulses technique utilizes the CMOS die-on-cuff to apply pulses to distinct contacts, thus fostering higher average charge density in the deeper tissues while maintaining a reduced charge density on the surface. This is achieved through the sequential activation of serval pairs (three in this example) of source/sink current sources, which facilitates building up the charge in the deep tissue. As a result, a cumulative charge in the deep tissue surpasses the recruitment threshold of the central fascicle (illustrated in green), without recruiting fascicles near the surface. The finite element method (FEM) simulation results in Fig. 4 (b) portray the electric field density across the nerve trunk, highlighting

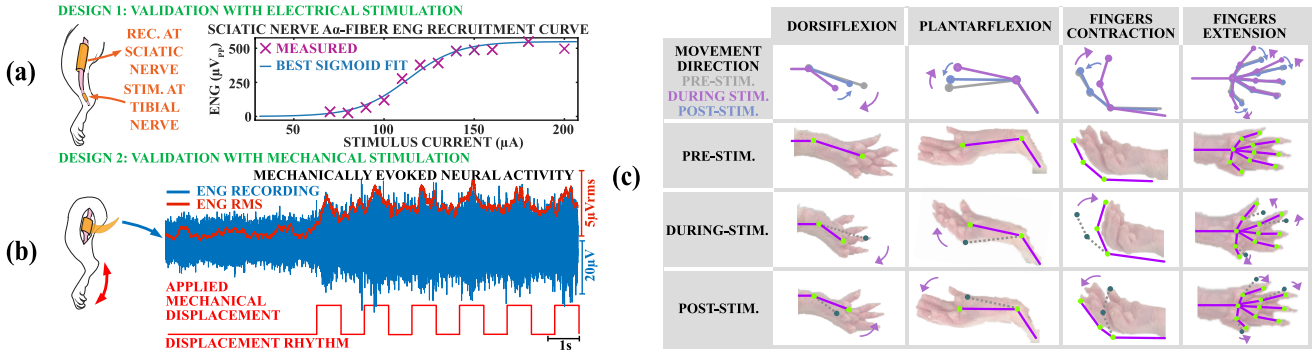

Fig. 5. In vivo validation in Wistar rats: (a) ENG signal amplitude response on the sciatic nerve to tibial nerve stimulation (the first design); (b) recorded compound action potentials in response to mechanical stimulation of a lower limb (the second design); and (c) in vivo demonstration of temporal interference stimulation in selective stimulation resulting in reaching one of the four states of a lower limb of a rat (the second design).

the selective recruitment when normalized electric field within the fascicles is considered.

Our second design adapts the TIS method from the brain [9] to the PNS, as displayed in Fig. 4 (c). This method utilizes two (or more) pairs of stimulation electrodes to deliver two differential high-frequency current stimulation signals with a slight frequency difference, Δf. These create two electric fields, E_1 and E_2, resulting in an intermodulation field where Δf is the frequency of the interference envelope. Fig. 4 (d) shows a circuit-based analysis of the TIS principle, modeling the electrode and tissue interface with a lumped component model, Z_{IN}. Two differential current sources correspond to frequencies of f_c and $f_c + \Delta f$, and their summation creates a low-frequency Δf modulation envelope most potent in the nerve's central region. A Nerve acts as a lowpass filter [18] and extracts this envelope. Adjusting the strength of each current source and stimulating electrode pairs allows for selective targeting within the nerve bundle, given nerves' reactivity in the lower frequency range where Δf exists. The selective stimulation of TIS, stimulating top-left, center, and bottom-right fascicles, is demonstrated via a FEM color map in Fig. 4 (e). In essence, ISP stimulation, with simple biphasic waveforms, is straightforward but less selective and effective at depth. Conversely, TIS offers deep, selective stimulation, but its complex high-frequency waveforms could complicate implementation, increase power usage and cause tissue to overheat. The choice between the two depends on factors like implant depth, and power limits.

IV. Measurement Results

A. Wireless powering and data communication

Our first design employs inductive power transmission. This choice attained a power efficiency of 1.1% through 4.5 mm muscle tissue [2]. The implanted module extracts 810 μW from a modest power of 74 mW supplied from the transmission source, ensuring adherence to the stipulated specific absorption rate safety constraints [19]. Our second design amalgamates synergies with ultrasonic energy harvesters, facilitating the wireless conveyance of power transdermally. The power supply route incorporates a full-wave bulk-biased passive rectifier succeeded by a low dropout regulator bank, demonstrating 70% power conversion efficiency of power shaping circuits (rectifier and LDO) under a load with a power consumption of 480μW [3]. The data transmitted to the implant chips is encoded into the wireless power using amplitude shift keying. This process involves modulating the amplitude of both inductive and ultrasound energy. In brief, both inductive and ultrasound wireless powering offer distinct benefits and drawbacks. Inductive power, safe and efficient, works best for short distances but struggles with longer distances, coil misalignment, and tissue penetration. Conversely, ultrasound power effectively reaches deeply implanted devices and can target specific areas but might cause tissue heating. The choice between these methods relies on device needs, implantation depth, and patient safety considerations.

B. In vivo validation in rodents

Both designs were subjected to in vivo validation involving Wistar rats. A 8×8-contact passive electrode array was surgically positioned over the sciatic nerve and interfaced with an IC as indicated in Figs. 5(a,b). For the first design (Fig. 5(a)), the tibial nerve was electrically stimulated to induce action potentials, which were then registered at the proximal segment of the sciatic nerve trunk. A nerve recruitment curve was formulated for biphasic current pulses up to 200μA.

For the second design (Fig. 5(b)), validation was achieved through mechanical stimulus by recording the compound action potentials elicited by the dorsiflexion of the rat's paw. Furthermore, the in vivo demonstration of TIS is shown in Fig. 5(c). Here, four unique movements of the rat's hind paw were induced by stimulating different electrode contact pairs, with an activity threshold maintained at 2V.

V. Conclusion

This paper has comprehensively illustrated and compared two advanced designs of PNS active neural interfaces, highlighting their pros and cons. The understanding derived from this synthesis provides a substantial platform for future advancements in the realm of neural interfaces, with potential implications for medical interventions and treatments related to nerve disorders.

References

[1] J. Galgani, C. Moro, and E. Ravussin, "Metabolic flexibility and insulin resistance," *AJP Endocrinology and Metabolism*, vol. 295, Aug. 2008. DOI: 10.1152/ajpendo.90558.2008.

[2] M. ElAnsary, J. Xu, J. de Sales Filho, G. Dutta, L. Long, A. Shoukry, C. Tejeiro, C. Tang, E. Kilinc, J. Joshi, P. Sabetian, S. Unger, J. Zariffa, P. Yoo, and R. Genov, "Multi-modal peripheral nerve active probe and microstimulator with on-chip dual-coil power/data transmission and 64 2nd-order opamp-less $\Delta\Sigma$ ADCs," Mar. 2021. DOI: 10.1109/ISSCC42613.2021.9365856.

[3] J. Xu, J. de Sales Filho, S. Nag, L. Long, C. Tejeiro, E. Hwang, G. O'Leary, Y. Huang, M. Kanchwala, M. Abdolrazzaghi, C. Tang, P. Liu, Y. Sui, X. Liu, G. Eleftheriades, J. Zariffa, and R. Genov, "Fascicle-selective bidirectional peripheral nerve interface IC with 173dB fom noise-shaping SAR ADCs and 1.38pj/b frequency-multiplying current-ripple radio transmitter," Feb. 2023, pp. 31–33. DOI: 10.1109/ISSCC42615.2023.10067626.

[4] S. Lawrence, G. Dhillon, and K. Horch, "Fabrication and characteristics of an implantable, polymer-based, intrafascicular electrode," *Journal of neuroscience methods*, vol. 131, pp. 9–26, Jan. 2004. DOI: 10.1016/S0165-0270(03)00231-0.

[5] C. Larson and E. Meng, "A review for the peripheral nerve interface designer," *Journal of Neuroscience Methods*, vol. 332, p. 108 523, Nov. 2019. DOI: 10.1016/j.jneumeth.2019.108523.

[6] K. Garde, E. Keefer, B. Botterman, P. Galvan, and M. Romero, "Early interfaced neural activity from chronic amputated nerves," *Frontiers in neuroengineering*, vol. 2, p. 5, Feb. 2009. DOI: 10.3389/neuro.16.005.2009.

[7] D. J. Tyler and D. M. Durand, "Chronic response of the rat sciatic nerve to the flat interface nerve electrode," *Annals of Biomedical Engineering*, vol. 31, no. 6, pp. 633–642, 2003.

[8] M. Vöröslakos, Y. Takeuchi, K. Brinyiczki, T. Zombori, A. Oliva, A. Fernández-Ruiz, G. Kozák, Z. T. Kincses, B. Iványi, G. Buzsáki, *et al.*, "Direct effects of transcranial electric stimulation on brain circuits in rats and humans," *Nature communications*, vol. 9, no. 1, pp. 1–17, 2018.

[9] N. Grossman, D. Bono, N. Dedic, S. Kodandaramaiah, A. Rudenko, H.-J. Suk, A. Cassara, E. Neufeld, N. Kuster, L.-H. Tsai, A. Pascual-Leone, and E. Boyden, "Noninvasive deep brain stimulation via temporally interfering electric fields," *Cell*, vol. 169, 1029–1041.e16, Jun. 2017. DOI: 10.1016/j.cell.2017.05.024.

[10] G. O'Leary, J. Xu, L. Long, J. S. Filho, C. Tejeiro, M. ElAnsary, C. Tang, H. Moradi, P. Shah, T. A. Valiante, and R. Genov, "A neuromorphic multiplier-less bit-serial weight-memory-optimized 1024-tree brain-state classifier and neuromodulation soc with an 8-channel noise-shaping SAR ADC array," *2020 IEEE International Solid- State Circuits Conference - (ISSCC)*, 2020, pp. 402–404. DOI: 10.1109/ISSCC19947.2020.9062962.

[11] M. R. Pazhouhandeh, G. O'Leary, I. Weisspapir, D. Groppe, X.-T. Nguyen, K. Abdelhalim, H. M. Jafari, T. A. Valiante, P. Carlen, N. Verma, and R. Genov, "Adaptively clock-boosted auto-ranging responsive neurostimulator for emerging neuromodulation applications," *2019 IEEE International Solid-State Circuits Conference - (ISSCC)*, 2019, pp. 374–376. DOI: 10.1109/ISSCC.2019.8662458.

[12] M. R. Pazhouhandeh, A. Amirsoleimani, I. Weisspapir, P. Carlen, and R. Genov, "Adaptively clock-boosted auto-ranging neural-interface for emerging neuromodulation applications," *IEEE Transactions on Biomedical Circuits and Systems*, vol. 16, no. 6, pp. 1138–1152, 2022. DOI: 10.1109/TBCAS.2022.3223988.

[13] H. Kassiri, R. Pazhouhandeh, N. Soltani, M. T. Salam, P. Carlen, J. L. P. Velazquez, and R. Genov, "All-wireless 64-channel 0.013mm2/ch closed-loop neurostimulator with rail-to-rail DC offset removal," *2017 IEEE International Solid-State Circuits Conference (ISSCC)*, ISSN: 2376-8606, Feb. 2017, pp. 452–453. DOI: 10.1109/ISSCC.2017.7870456.

[14] H. Kassiri, M. T. Salam, M. R. Pazhouhandeh, N. Soltani, J. L. Perez Velazquez, P. Carlen, and R. Genov, "Rail-to-rail-input dual-radio 64-channel closed-loop neurostimulator," *IEEE Journal of Solid-State Circuits*, vol. 52, no. 11, pp. 2793–2810, Nov. 2017, Conference Name: IEEE Journal of Solid-State Circuits, ISSN: 1558-173X. DOI: 10.1109/JSSC.2017.2749426.

[15] R. Koh, M. Balas, A. Nachman, and J. Zariffa, "Selective peripheral nerve recordings from nerve cuff electrodes using convolutional neural networks," *Journal of Neural Engineering*, vol. 17, Oct. 2019. DOI: 10.1088/1741-2552/ab4ac4.

[16] M. ElAnsary, J. Xu, J. de Sales Filho, G. Dutta, L. Long, C. Tejeiro, A. Shoukry, C. Tang, E. Kilinc, J. Joshi, P. Sabetian, S. Unger, J. Zariffa, P. Yoo, and R. Genov, "Bidirectional peripheral nerve interface with 64 second-order opamp-less $\Delta\Sigma$ ADCs and fully integrated wireless power/data transmission," *IEEE Journal of Solid-State Circuits*, vol. 56, pp. 1–1, Nov. 2021. DOI: 10.1109/JSSC.2021.3113354.

[17] Y. E. Hwang, R. Genov, and J. Zariffa, "Resource-efficient neural network architectures for classifying nerve cuff recordings on implantable devices," *bioRxiv*, 2022. DOI: 10.1101/2022.10.05.510983. eprint: https://www.biorxiv.org/content/early/2022/10/07/2022.10.05.510983.full.pdf. [Online]. Available: https://www.biorxiv.org/content/early/2022/10/07/2022.10.05.510983.

[18] M. Bikson, M. Inoue, H. Akiyama, J. Deans, J. Fox, H. Miyakawa, and J. Jefferys, "Effect of uniform extracellular DC electric fields on excitability in rat hippocampal slices in vitro," *The Journal of physiology*, vol. 557, pp. 175–90, May 2004. DOI: 10.1113/jphysiol.2003.055772.

[19] N. Soltani, M. ElAnsary, J. Xu, J. S. Filho, and R. Genov, "Safety-optimized inductive powering of implantable medical devices: Tutorial and comprehensive design guide," *IEEE Transactions on Biomedical Circuits and Systems*, vol. 15, no. 6, pp. 1354–1367, 2021. DOI: 10.1109/TBCAS.2021.3125618.

[20] H. You, A. Amirsoleimani, J. Xu, M. Rahimi Azghadi, and R. Genov, "A subranging nonuniform sampling memristive neural network-based analog-to-digital converter," *Memories - Materials, Devices, Circuits and Systems*, vol. 4, p. 100 038, Mar. 2023. DOI: 10.1016/j.memori.2023.100038.

[21] A. Amirsoleimani, F. Alibart, V. Yon, J. Xu, M. Pazhouhandeh, S. Ecoffey, Y. Beilliard, R. Genov, and D. Drouin, "In-memory vector-matrix multiplication in monolithic complementary metal–oxide–semiconductor-memristor integrated circuits: Design choices, challenges, and perspectives," *Advanced Intelligent Systems*, vol. 2, p. 2 000 115, Aug. 2020. DOI: 10.1002/aisy.202000115.

[22] T. Liu, A. Amirsoleimani, J. Xu, F. Alibart, Y. Beilliard, S. Ecoffey, D. Drouin, and R. Genov, "Codex: Stochastic encoding method to relax resistive crossbar accelerator design requirements," *IEEE Transactions on Circuits and Systems II: Express Briefs*, vol. 69, Mar. 2022. DOI: 10.1109/TCSII.2022.3157789.